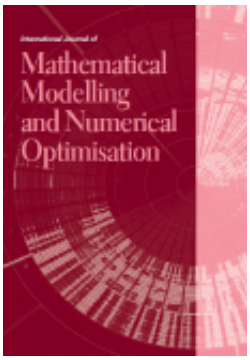

International Journal of Mathematical Modelling and Numerical Optimisation

ISSN online: 2040-3615 - ISSN print: 2040-3607
https://www.inderscience.com/ijmmno

Numerical modelling of wave propagation in shallow water

Vetrichelvan Pugazendi, Efstratios L. Ntantis

DOI: 10.1504/IJMMNO.2025.10073051

Article History:

Received:	01 April 2025
Last revised:	17 May 2025
Accepted:	11 June 2025
Published online:	29 August 2025

Numerical modelling of wave propagation in shallow water

Vetrichelvan Pugazendi

Cranfield University,
College Rd., Wharley End,
Bedford MK43 0AL, UK
Email: vetrichelvan1369@gmail.com

Efstratios L. Ntantis*

Amity University Dubai,
International Academic City,
Dubai 345019, UAE
Email: entantis@amityuniversity.ae
*Corresponding author

Abstract: Coastal communities worldwide face significantly higher risks than their inland counterparts, primarily due to threats like tsunamis, dam failures, and storm surges. Identifying and addressing these hazards before they result in loss of life is paramount. This paper presents a numerical scheme developed in MATLAB to solve shallow water equations, offering a valuable tool for mitigating these critical threats. Traditionally, computational limitations in memory and speed have required the division of complex simulations into smaller, more manageable sections in computational fluid dynamics. While advancements in computational power have grown exponentially, so too has the complexity of the problems being addressed. The model employs finite difference methods to solve the shallow water equations, utilising user-defined parameters such as domain size, shape, grid resolution, and boundary conditions. It generates customised data and presents results through animated visualisations. The results from this model have shown promising potential, highlighting its ability to enhance understanding and mitigation strategies for coastal hazards significantly.

Keywords: coastal hazards; coastal fluid dynamics; mitigation strategies; shallow water equations; MATLAB simulation.

Reference to this paper should be made as follows: Pugazendi, V. and Ntantis, E.L. (2025) 'Numerical modelling of wave propagation in shallow water', *Int. J. Mathematical Modelling and Numerical Optimisation*, Vol. 15, No. 5, pp.1–15.

Biographical notes: Vetrichelvan Pugazendi holds a BSc (Hons) in Aeronautical Engineering, as well as an MSc in Computational and Software Techniques in Engineering with a specialisation in computational engineering design from Cranfield University. He currently works as a CFD Engineer at a fire engineering firm, where he applies advanced simulation techniques to model fire dynamics and support safety-driven design solutions.

Efstratios L. Ntantis is a Mechanical Engineer specialising in Aerospace, bringing over 15 years of academic experience. He completed his PhD in Gas Turbine Performance Diagnostics at Cranfield University in the UK. His expertise spans various areas, including aerodynamic optimisation, thermo-fluid dynamics, sustainable flight, and space engineering. He is a member of the American Society of Mechanical Engineers (ASME), the Royal Aeronautical Society (RAeS), and the Technical Chamber of Greece (TEE).

1 Introduction

Ocean waves play a vital role in daily life, influencing everything from weather forecasting to climate modelling (Mendez and Rueda, 2008). They significantly impact weather predictions by modulating surface friction and enhancing the accuracy of hurricane intensity forecasts. Extreme ocean waves also pose a threat to coastal communities and offshore industries (Mendez et al., 2008). Waves propagate from deepwater to shallow regions. This paper focuses specifically on the shallow-water region, typically defined as areas where wave propagation occurs in depths of less than 1,000 feet (304 metres). In contrast, deep water is generally considered to be over 4,000 feet (1,219 metres) deep. The depth-to-wavelength ratio (h/L) characterises the transition from deep to shallow waves. Waves in deep water have an h/L ratio greater than 1/2, while transitional waves fall between 1/2 and 1/20. Waves with an h/L ratio of less than 1/20 are considered shallow water waves (Balitsky, 2019). As waves move from deep to shallow waters, their height increases while their speed decreases. This slowdown occurs because the shallower depth affects the wave's energy and momentum, leading to a rise in steepness and eventually causing the wave to break. The reduction in speed results from the water's shallower depth, which impacts the wave's energy distribution. As the velocity decreases, the wave height increases in compensation to conserve energy. Figure 1 presents a schematic model of wave-coast interaction, along with the corresponding formulas.

Wave propagation has been the subject of extensive research, with the foundational equations governing wave motion derived from the principles of conservation of mass, momentum, and energy. These equations can be adapted into different forms depending on assumptions related to fluid viscosity, compressibility, and domain characteristics (Stastna and Steinmoeller, 2023). However, a careful selection of assumptions is necessary to achieve accurate simulation results. Water movement is often described by shallow water equations, which are based on fluid mechanics principles and assume that the fluid is inviscid and incompressible. Shallow water flows are characterised by regions where free surfaces exist, and the primary flow component is typically horizontal velocity. Gravitational forces play a crucial role in generating stress on these free surfaces. The shallow water equations have broad applications in several critical fields, including tsunami propagation, river flows, dam breaks, and storm surges (Kumar et al., 2022).

The propagation of tsunamis poses a significant threat to coastal regions worldwide, prompting extensive efforts in detection, forecasting, and emergency preparedness to minimise loss of life and mitigate damage. A key component in understanding and predicting tsunami behaviour is the use of shallow water equations, which model the

complex dynamics of wave propagation. These equations enable more accurate predictions of wave height, speed, and arrival times, which help identify at-risk areas and support the implementation of targeted evacuation plans and early warning systems. Furthermore, they provide critical insights into the potential impact on infrastructure and ecosystems, informing strategies to enhance coastal resilience and preparedness against future tsunami events.

Shallow water equations for river flows are a powerful tool for accurately modelling river flow patterns and water levels, making them essential for analysing flow dynamics in various environments. These equations predict flood risks and identify vulnerable areas by capturing water movement across multiple terrains and accounting for slope and surface friction factors. This modelling capability is crucial for flood management, urban planning, and the design of flood control infrastructure. Moreover, it aids in assessing the effectiveness of mitigation strategies, enabling better preparation and response to potential flooding events.

Catastrophic dam failures can result in massive loss of life and extensive damage to infrastructure, driven by high-speed flows and shockwaves that propagate rapidly through affected areas. These events can lead to flash floods, overwhelming communities and causing irreparable harm. Researchers such as Roberts and Zoppou (2003) utilise shallow water equations to simulate the sudden and violent collapse of dams, providing critical insights into the behaviour of floodwaters and their resulting impact on downstream regions. This modelling is crucial for enhancing emergency response strategies, designing resilient infrastructure, and mitigating the overall risk of such disasters.

Modelling storm surges, driven by wind, atmospheric pressure, and tidal forces, is critical for accurately assessing coastal risks. This modelling helps inform early warning systems and guides the development of effective mitigation strategies, ensuring better preparedness to protect lives, property, and infrastructure from the devastating impacts of these extreme events.

Figure 1 Wave transformation from deep to shallow water (see online version for colours)

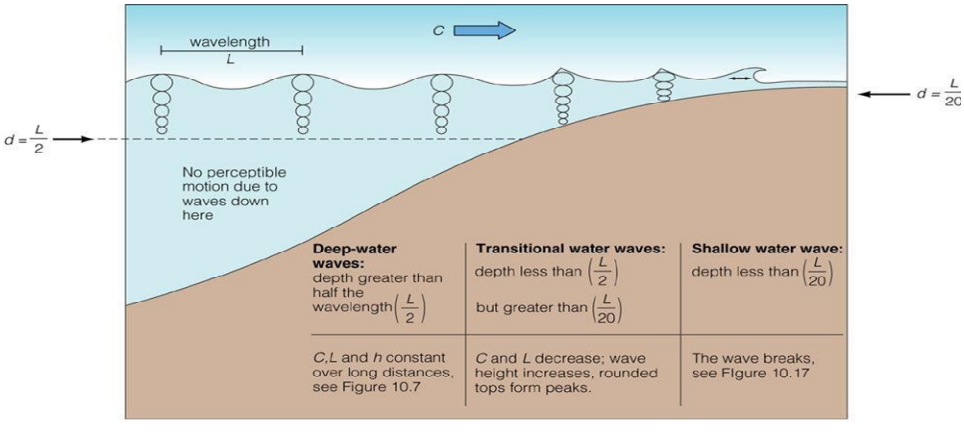

Source: Balitsky (2019)

Several numerical methods are available for solving shallow water equations, including the finite difference and finite element methods. This study focuses specifically on the finite difference method. This approach involves selecting computational points and

determining their spacing, which is the foundation for applying a finite difference approximation scheme. The process then computes the equations across the domain at each timestep. When modelling any problem, making informed and sensible decisions regarding the selection of appropriate initial and boundary conditions for the specific scenario is crucial. This study models the inlet boundary condition by a sinusoidal wave. In contrast, the outlet boundary conditions are adaptable, allowing for either wave reflection or absorption based on user input. The primary goal of this research is to develop a code capable of conducting three-dimensional numerical simulations of shallow water equations, offering users the flexibility to define and manipulate key parameters such as domain size, wave characteristics, and boundary conditions.

2 Mathematics and numerical methods

Fluid mechanics, the study of fluid motion, offers a comprehensive framework for understanding and modelling a wide range of flow phenomena. The governing equations that describe fluid behaviour are rooted in the fundamental principles of mass, momentum, and energy conservation. These equations provide the mathematical foundation for analysing the behaviour of fluids under various conditions. The specific flow scenario examined in this paper closely aligns with real-world phenomena observed in coastal regions, where dynamic interactions between water and the environment give rise to complex fluid behaviours. This study extends beyond theoretical analysis, addressing practical challenges in coastal engineering, environmental management, and disaster preparedness, where fluid dynamics play a crucial role in understanding wave propagation, flooding, and other critical processes. By leveraging these principles, the research aims to contribute to a deeper understanding of fluid behaviour and inform solutions to pressing issues in coastal and hydrodynamic systems.

2.1 Mass conservation equations

The mass conservation equation states that the mass of fluid within a control volume remains constant over time, Δt. For a fixed control volume bounded by surfaces of dimensions dx, dy, dz along the x, y, and z axes, the mass of the fluid at time t is $\rho dxdydz$. After a time interval Δt, the mass of the fluid changes to $\left(\rho + \frac{\partial \rho}{\partial t} dt\right) dxdydz$. The fluid's mass change is described as in equation (1), (Ge et al, 2024).

$$\rho dxdydz - \left(\rho + \frac{\partial \rho}{\partial t} dt\right) dxdydz = -\frac{\partial \rho}{\partial t} dtdxdydz \tag{1}$$

The fluid mass entering the control volume at time Δt is given by $\rho udxdydzdt$, and the mass of the fluid leaving the control volume at time Δt is provided by $\left(\rho u + \frac{\partial \rho u}{\partial t} dxdydzdt\right)$. The difference in fluid mass entering and leaving the control volume at time Δt in the x-direction is given by equation (2) in (Crowhurst and Li, 2013).

$$x - direction \quad \rho udxdydzdt - \left(\rho u + \frac{\partial \rho u}{\partial x}\right) dxdydzdt = -\frac{\partial \rho u}{\partial x} dxdydzdt \tag{2}$$

Similarly, the difference in fluid mass entering and leaving the control volume at time Δt in the y-direction and z-direction is expressed by equation (3) and equation (4).

$$y-direction\ -\frac{\partial \rho v}{\partial y}dxdydzdt \tag{3}$$

$$z-direction-\frac{\partial \rho w}{\partial z}dxdydzdt \tag{4}$$

The total change in fluid mass in the control volume at time Δt is shown in equation (5).

$$-\left(\frac{\partial \rho u}{\partial x}+\frac{\partial \rho v}{\partial y}+\frac{\partial \rho w}{\partial z}\right)dxdydzdt \tag{5}$$

Combining equations (1) and (2), the mass continuity equation for three-dimensional unsteady compressible flows is given in equation (6).

$$\frac{\partial \rho}{\partial t}+\frac{\partial \rho u}{\partial x}+\frac{\partial \rho v}{\partial y}+\frac{\partial \rho w}{\partial z}=0 \tag{6}$$

In this study, the fluid is assumed to be incompressible, meaning its density remains constant; therefore, the density gradient is zero. This simplification transforms the continuity equation into a volume conservation equation, as presented in equation (7).

$$\frac{\partial \rho u}{\partial x}+\frac{\partial \rho v}{\partial y}+\frac{\partial \rho w}{\partial z}=0 \tag{7}$$

2.2 Equations of motion

The equations of motion arise from Newton's second law of motion, which states that the force equals the rate of change of momentum over time. In fluid mechanics, these forces can include shear or tangential forces caused by fluid viscosity and gravitational effects within the control volume. The pressure exerted in the x-direction within a control volume is calculated by equation (8) (Li, 2024).

$$F_{xp}=-\frac{\partial P}{\partial x}dxdydz \tag{8}$$

Shear and tangential forces in the x-direction in a control volume can be determined by equations (9) and (10), (Oliver, 1998).

$$F_{xs}=\delta_{xx}-\left(\delta_{xx}+\frac{\partial \delta_{xx}}{\partial x}dx\right)dydz+\left(\tau_{yx}+\frac{\partial \tau_{yx}}{\partial y}dy\right)dxdz+\left(\tau_{zx}+\frac{\partial \tau_{zx}}{\partial z}dz\right)dxdy \tag{9}$$

$$F_{xs}=\left(\frac{\partial \delta_{xx}}{\partial x}+\frac{\partial \tau_{yx}}{\partial y}+\frac{\partial \tau_{zx}}{\partial z}\right)dxdydz \tag{10}$$

Each face of the control volume experiences one normal stress δ, and two shear stresses τ. The following relationship is derived from Newton's second law of motion.

$$F_{xs}=M\times A_x \tag{11}$$

where M is the mass flow rate in the control volume given by $\rho dxdydz$; A_x is the acceleration of the fluid in the x-direction given by $\frac{du}{\partial t}$; u is a function of $u(x, y, z, t)$.

$$A_x = \frac{\partial u(x, y, z, dt)}{\partial t} \tag{12}$$

$$A_x = \frac{\partial u}{\partial t} + u\frac{\partial u}{\partial x} + v\frac{\partial u}{\partial y} + w\frac{\partial u}{\partial z} \tag{13}$$

The terms $u\frac{du}{dx}$, $v\frac{du}{dy}$, $w\frac{du}{dz}$, are known as the convective acceleration terms and account for the change in velocity at a given time concerning distance; the term $\frac{du}{dt}$ is known as the local acceleration term, which accounts for the change in velocity at a given distance concerning time. The total force acting on the control volume in the x-direction is given by equation (14), (Cheviakov and Zhao, 2024).

$$F_x = \left(-\frac{\partial P}{\partial x} + \frac{\partial \delta_{xx}}{\partial x} + \frac{\partial \tau_{yx}}{\partial y} + \frac{\partial \tau_{zx}}{\partial z} + X \right) dxdydz \tag{14}$$

From equations (12) and (14), the relationship can be derived as follows:

$$\rho\left(\frac{du}{dt} + u\frac{du}{dx} + v\frac{du}{dy} + w\frac{du}{dz} \right) = -\frac{\partial P}{\partial x} + \frac{\partial \delta_{xx}}{\partial x} + \frac{\partial \tau_{yx}}{\partial y} + \frac{\partial \tau_{zx}}{\partial z} + X \tag{15}$$

The sum of pressure and viscous forces is proportional to the coefficient of shear stress and linear deformation, while normal forces are a function of the coefficient of angular deformation. These principles yield the Navier-Stokes equations in the x-direction (see equation (16)), y-direction (see equation (17)), and z-direction (see equation (18)) as provided below (Lyons, 2014).

$$\rho\left(\frac{\partial u}{\partial t} \right) = \rho\left(\frac{\partial u}{\partial t} + u\frac{du}{\partial x} + v\frac{du}{\partial y} + w\frac{du}{\partial z} = -\frac{\partial P}{\partial x} + \mu\nabla^2 u \right) \tag{16}$$

$$\rho\left(\frac{\partial v}{\partial t} \right) = \rho\left(\frac{\partial v}{\partial t} + u\frac{dv}{\partial x} + v\frac{dv}{\partial y} + w\frac{dv}{\partial z} = -\frac{\partial P}{\partial x} + \mu\nabla^2 v \right) \tag{17}$$

$$\rho\left(\frac{\partial w}{\partial t} \right) = \rho\left(\frac{\partial w}{\partial t} + u\frac{dw}{\partial x} + v\frac{dw}{\partial y} + w\frac{dw}{\partial z} = -\frac{\partial P}{\partial x} + \mu\nabla^2 w \right) \tag{18}$$

2.3 Shallow water equations

The shallow water equations can be derived from the shallow water wave theory. Shallow water wave theory assumes that the depth is much smaller than the wavelength and the hydrostatic pressure. The pressure is considered to be constant everywhere (Augier et al., 2019).

$$P = 0$$

Fluid on the surface with its velocity components u, v at a time Δt must satisfy the changes in its position $z = \eta(x, y, t)$, (Augier et al., 2019).

$$dz = \frac{\partial \eta}{\partial t} dt + \frac{\partial \eta}{\partial x} dx + \frac{\partial \eta}{\partial y} dy \tag{19}$$

$$w = \frac{\partial \eta}{\partial t} + u \frac{\partial \eta}{\partial x} + v \frac{\partial \eta}{\partial y} \tag{20}$$

The component along z from Euler's equation is considered gravity.

$$\frac{dw}{dt} = \frac{\partial w}{\partial t} + u \frac{\partial w}{\partial x} + v \frac{\partial w}{\partial y} + w \frac{\partial w}{\partial z} = -\frac{1}{\rho} \frac{\partial P}{\partial z} - g \tag{21}$$

The vertical acceleration term $\left(\frac{\partial w}{\partial t} \right)$ is neglected since the value is minimal compared to the horizontal component (Hedley, 2009).

$$\begin{gathered} -\rho g - \frac{\partial P}{\partial z} = 0 \Rightarrow \\ -\int \rho g dz - \int \frac{\partial P}{\partial z} dz = 0 \Rightarrow \\ P = -\rho g z + C \end{gathered} \tag{22}$$

Applying boundary conditions the equation (22) turns into:

$$P = -\rho g z + \rho g \eta = \rho g (\eta - z) \tag{23}$$

Substituting for pressure in the x component of Euler's equation gives equation (24), (Carrier and Yeh, 2005).

$$\frac{du}{dt} = -\rho g \frac{\partial \eta}{\partial x} \tag{24}$$

Integrating the continuity equation for depth in the x-direction yields:

$$\int_{-d}^{\eta} \left(\frac{\partial u}{\partial x} + \frac{\partial w}{\partial z} \right) dz = 0 \tag{25}$$

Getting the shallow water equation:

$$\frac{\partial \eta}{\partial t} + \frac{\partial}{\partial x} \int_{-d}^{\eta} u dz + u \frac{\partial \eta}{\partial x} = 0 \tag{26}$$

The equations (24) and (26) are known as shallow water equations, (Maatoug and Ayadi, 2016).

2.4 Boussinesq equation

The Boussinesq equation, as expressed in equation (27), simplifies fluid flow analysis by assuming that the vertical component of velocity increases linearly from the bed to the surface, neglecting the small convective terms in kinematic conditions (Chen and Liu,

1995). This assumption reduces the complexity of the problem by approximating the vertical velocity profile in a way that explicitly eliminates the need to account for variations in velocity at different depths. Additionally, the equation neglects the small convective terms in the kinematic boundary conditions. It is a valuable approximation for flows where vertical velocity gradients are relatively small and the horizontal flow dominates. This simplification is especially effective in shallow water flow scenarios, where the primary focus is on the horizontal movement of water, and vertical variations in velocity are assumed to be minimal. While this approximation may not be universally applicable in all fluid dynamics problems, it provides a practical solution for modelling certain types of flow, particularly in coastal and riverine environments.

$$w = \frac{dh}{dt} = \frac{\partial h}{\partial t} \tag{27}$$

Using the assumption:

$$w(z) = \frac{\partial h}{\partial t}\frac{z}{h} \tag{28}$$

Neglecting the convective terms from Euler's equation:

$$\frac{\partial w}{\partial t} = -\frac{1}{\rho}\frac{\partial P}{\partial z} - g \tag{29}$$

Accounting for the vertical distribution:

$$\frac{z}{h}\frac{\partial^3 h}{\partial t^3} = -\frac{z}{h^2}\left(\frac{\partial h}{\partial t}\right)^2 = -\frac{1}{\rho}\frac{\partial P}{\partial z} - g \tag{30}$$

Neglecting the power of derivatives:

$$\frac{z}{h}\frac{\partial^3 h}{\partial t^3} = -\frac{1}{\rho}\frac{\partial P}{\partial z} - g \tag{31}$$

Integrating from the point of $P = 0$ to z to obtain the pressure distribution (Whitham, 1974):

$$\frac{1}{\rho}\int_z^h \frac{\partial P}{\partial z}dz = -g\int_z^h dz - \int_z^h \frac{z}{h}\frac{\partial^2 h}{\partial t^2}dz \Rightarrow \frac{P}{\rho} = -\rho g(h-z) - \frac{h^2 - z^2}{zh}\rho\frac{\partial^2 h}{\partial t^2} \tag{32}$$

Substituting the pressure distribution in the Euler equation:

$$\frac{\partial u}{\partial t} = -g\frac{\partial (h-z)}{\partial x} - \left(\frac{\partial^3 h}{\partial x \partial t^2}\frac{h^2 - z^2}{2h}\right) - \left(\frac{\partial^2 h}{\partial x \partial t}\frac{\partial}{\partial x}\left(\frac{h^2 - z^2}{2h}\right)\right) \tag{33}$$

Neglecting derivative products, following the Boussinesq equation:

$$\frac{\partial u}{\partial t} + g\frac{\partial h}{\partial x} = -\frac{1}{3}\frac{\partial^3 h}{\partial x \partial t^2} \tag{34}$$

2.5 Numerical method

The finite difference approximation of partial differential terms in equations aims to solve them numerically. However, since it involves approximation, errors can arise during computation. The scheme becomes increasingly unstable as errors accumulate with larger timesteps (Lighthill. 2005). Therefore, assessing stability and accuracy is crucial when employing finite difference schemes. The discrepancy between the solution obtained through finite differences and the actual solution is called the truncation error. Reducing the spatial and temporal step sizes or employing Taylor series expansions can minimise the *truncation error*. Taylor series expansion for $f(x + \Delta x)$ can be written as follows (Bosa and Petti, 2010; Broomans, 2003).

$$f(x+\Delta x) = f(x) + \Delta x \frac{\partial f}{\partial x} + \frac{\Delta x^2}{2!}\frac{\partial^2 f}{\partial x^2} + \frac{\Delta x^3}{3!}\frac{\partial^3 f}{\partial x^3} + \cdots \tag{35}$$

$$\frac{\partial f}{\partial x} = \frac{f(x+\Delta x) - fx}{(\Delta x)} - \frac{\Delta x}{2!}\frac{\partial^2 f}{\partial x^2} - \frac{\Delta x^2}{3!}\frac{\partial^3 f}{\partial x^3} - \cdots \tag{36}$$

In finite difference form, the forward differencing is written as:

$$\frac{\partial f}{\partial x} = \frac{f_{i+1} - f_i}{(\Delta x)} \tag{37}$$

Similarly, using the Taylor series to expand $f(x–\Delta x)$ and rearranging leads to backward differencing, which is written as:

$$\frac{\partial f}{\partial x} = \frac{f_i - f_{i-1}}{(\Delta x)} \tag{38}$$

Central differencing can be obtained by subtracting forward and central differencing schemes.

$$\frac{\partial f}{\partial x} = \frac{f_{i+1} - f_{i-1}}{2(\Delta x)} \tag{39}$$

Correspondingly, solving for horizontal and vertical velocity components for the shallow water equations leads to equations (40) and (41) (Broomas, 2003; Welahettige et al., 2018).

$$u_{i,j}^{n+1} = u_{i,j}^{n} - g\frac{\Delta t}{\Delta x}\left(n_{i+i,j}^{n} - n_{i-i,j}^{n}\right) \tag{40}$$

$$v_{i,j}^{n+1} = v_{i,j}^{n} - g\frac{\Delta t}{\Delta x}\left(n_{i,j+1}^{n} - n_{i,j-1}^{n}\right) \tag{41}$$

Similarly, solving for the wave height for the shallow water equations leads to equation (42) (Broomans, 2003).

$$n_{i,j}^{n+1} = 2\times n_{i,j}^{n} - n_{i,j}^{n-1} + \left(\frac{2\Delta t^2}{\Delta x \Delta v}\times\left(n_{i+i,j}^{n} + n_{i-1,j}^{n} + n_{i,j+1}^{n} - 4\times n_{i,j}^{n}\right.\right. \tag{42}$$

The sponge layer criterion is introduced once the wave has propagated to 75% of the domain length. At this point, the wave-dampening function is applied to mitigate wave reflections (see Table 1). This technique helps to prevent spurious reflections at the boundaries that could distort the simulation results. The sponge layer gradually absorbs the wave energy, ensuring the wave does not artificially bounce back into the computational domain. By applying the wave-dampening function in a controlled manner, the sponge layer effectively simulates the natural dissipation of energy that would occur in real-world conditions, contributing to a more accurate representation of wave behaviour and enhancing the overall stability of the numerical model.

Table 1 Boundary conditions

Boundary condition	*Function*
Inlet	$Z = A \times \sin\left(\sqrt{x^2 + y^2} + \varnothing\right.$
Outlet	Reflective or sponge layer

3 Code development and testing

For this study, MATLAB was selected for its efficient and robust computational environment. It performs complex mathematical calculations, analyses, and optimisations with remarkable speed, accuracy, and precision. By treating all variables as matrices, MATLAB facilitates seamless matrix operations. Additionally, the symbolic toolbox allows for straightforward calculus computations when needed. The graphical interface is user-friendly and easy to program, enhancing workflow efficiency. MATLAB also provides various functions for visualising results, ensuring aesthetic quality and high precision. In addition, MATLAB code is compatible across multiple versions of the software.

4 Results and discussion

To evaluate wave behaviour over time, Figure 2(a) plots the maximum wave height against timestep based on numerical methods, while Figure 2(b) illustrates wave amplitude versus wavelength using an analytical sine wave under the absorption boundary outlet condition. Initially, the maximum wave height within the domain corresponds closely to the analytical solution. As the simulation advances, gravitational effects embedded in the numerical model gradually reduce the wave height. The sponge layer parameters outlined in Table 1 also contribute to this damping behaviour. When the wave reaches 75% of the domain width, the sponge layer becomes active, further suppressing wave propagation. To accelerate convergence, wave heights that decay to negligible values are approximated as zero. By $t = 90$, the wave height stabilises at zero, indicating convergence of the simulation. Upon convergence, a *'simulation complete*' dialog box appears. If convergence is not achieved, an '*incomplete*' dialog recommends adjusting the timestep to improve results.

Figure 2 Maximum wave height using (a) numerical method and (b) analytical sinusoidal wave (see online version for colours)

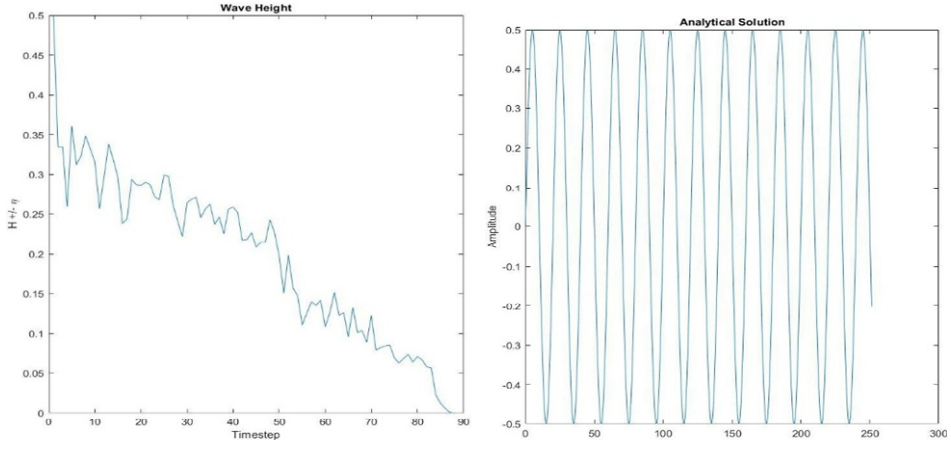

(a) (b)

Figure 3 Max wave height vs. timestep from (a) numerical method for RBOC (b) max wave height from analytical sinusoidal wave for RBOC (see online version for colours)

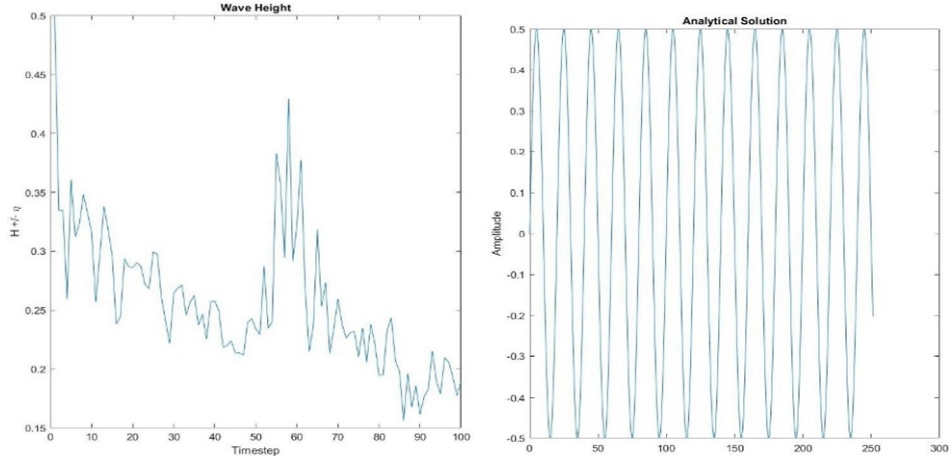

(a) (b)

In addition, Figure 3(a) illustrates the maximum wave height over a timestep, calculated using numerical methods under a reflective boundary outlet condition for Risk-Based Optimal Control (RBOC). As the wave moves through the domain, its height gradually decreases. Upon reaching the boundary, the wave height increases due to accumulation against the outlet, followed by reflection back into the domain. In contrast, Figure 3(b) presents the analytical sine wave solution for RBOC, which maintains a constant wave height throughout. This idealised model omits external influences such as gravity, whereas the numerical simulation accounts for these effects. As a result, while the initial wave height matches the analytical solution, deviations emerge during propagation due to gravitational and other external factors.

Figure 4 Initial timestep simulation of absorption boundary (see online version for colours)

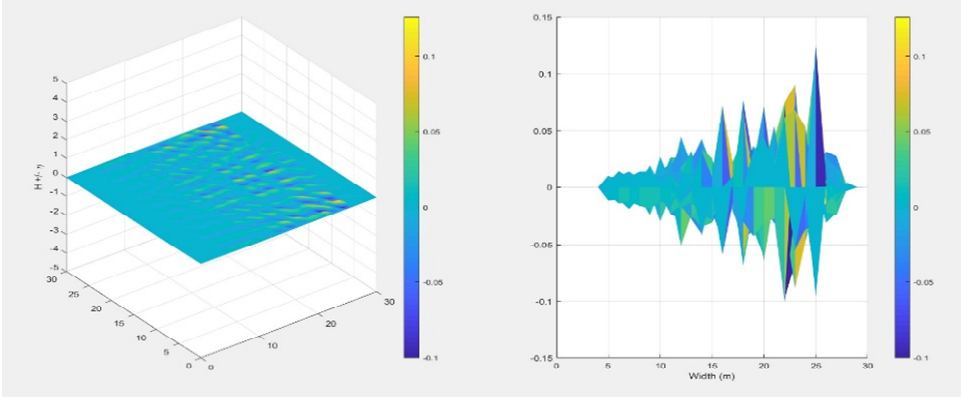

Figure 5 Final timestep simulation of absorption boundary with sponge layer criteria (see online version for colours)

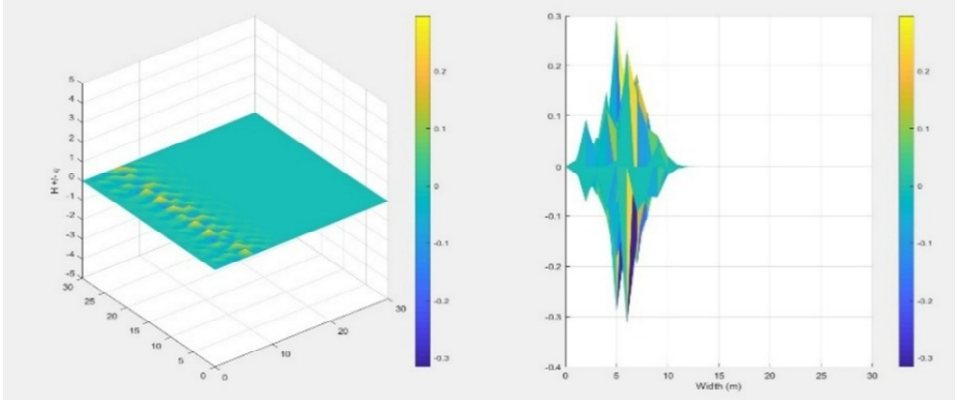

Figures 4 and 5 demonstrate simulations conducted under the absorption boundary outlet condition. These figures illustrate the propagation of waves through the domain at different time steps: Figure 4, at an earlier time, and Figure 5, at a later time. Figure 4 shows that as the wave reaches 23 m, there is a noticeable decrease in wave height due to the sponge layer criteria, which initiates damping when the wave reaches 75% of the domain length (23 m out of 30 m).

Plots in Figures 6 and 7 present the reflective boundary outlet condition, where the wave reflects after reaching the outlet, as expected. Figures 4 to 7 are computed for the specified domain size and plotted against the wave height calculated using numerical methods. The right side plots of Figures 4 and 5 provide a side view of the wave simulation, clearly showing the damping effect on wave height. In contrast, the right side plots of Figures 6 and 7 present a top view, emphasising the reflection effect at the outlet. These perspectives are chosen for visualisation purposes. Notably, no wave height damping is observed when the reflective boundary outlet condition is applied.

Figure 6 Initial timestep simulation of reflective boundary (see online version for colours)

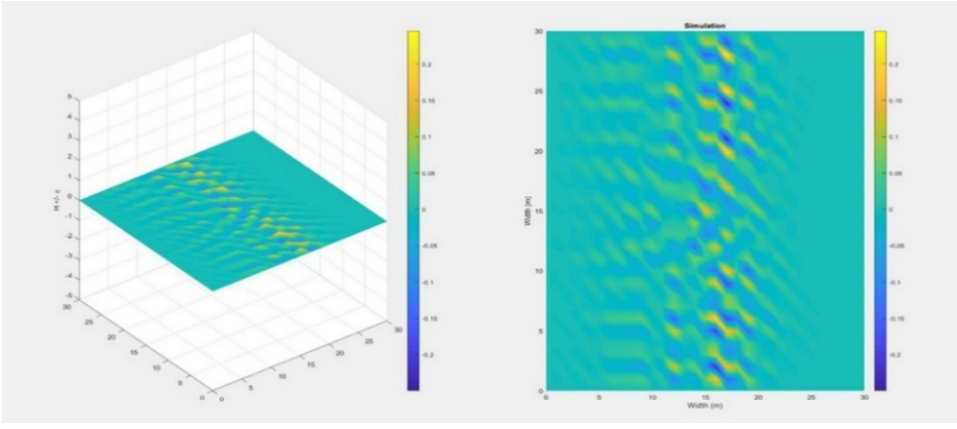

Figure 7 Final timestep simulation of reflective boundary (see online version for colours)

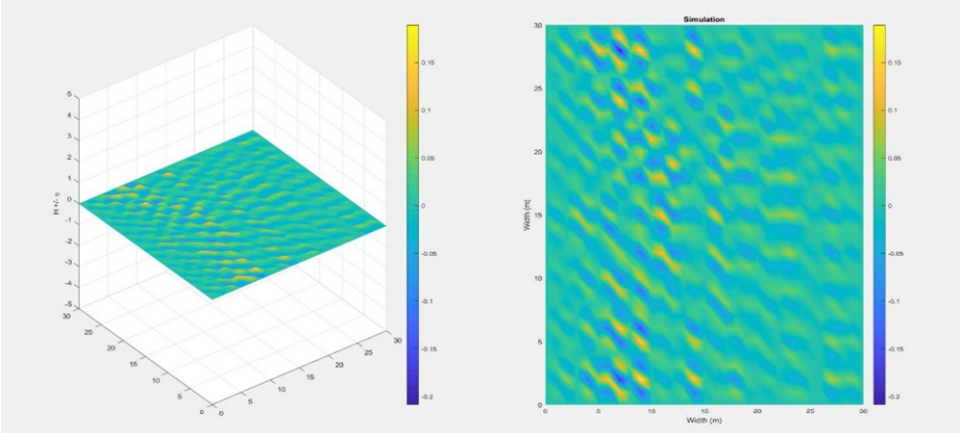

5 Conclusions

The paper uses user-defined data to present a MATLAB-based code developed for the three-dimensional numerical simulation of shallow water equations. The code employs the Finite Difference method, which necessitates selecting computational grid points and their spacing. Once these parameters are defined, a finite difference approximation scheme is applied to solve the equations over the domain at various time steps. The inlet boundary condition used in this study is a sinusoidal wave, while the outlet boundary conditions can be either reflective or absorbing, based on user input. The code generates an animated plot that visually demonstrates the wave dynamics. For reflective boundary conditions, the animation displays wave propagation and reflection from the outlet wall, continuing until the specified number of time steps is completed. For absorbing boundary conditions, the wave's height diminishes as it reaches 75% of the domain length, and the simulation alerts the user upon complete dampening within the designated time steps. An

incomplete simulation alert is issued if the wave does not thoroughly dampen. Future work will focus on enhancing the accuracy of the numerical schemes, as greater accuracy is crucial for addressing more complex problems. Improving the computer's processor efficiency is essential for handling more significant issues or real-world scenarios. Future enhancements could also include integrating bed slope variations into the simulation, investigating different bed slope sizes, and analysing wave breakpoints, which are critical for subsequent research. Furthermore, examining the accuracy and stability of various numerical schemes will be an essential area of study.

Declarations

Data availability does not apply to this article as no new data were created or analysed in this study.

This study was not supported by any sponsor or funder.

The authors declare that they have no conflicts of interest, whereas no scientific funding is involved.

This study does not require ethical approval.

Authors declare no any competing financial and/or non-financial interests.

References

Augier, P, Mohanan A.V. and Lindborg E. (2019) 'Shallow water wave turbulence', *Journal of Fluid Mechanics*, Vol. 874, pp.1169–196, DOI:10.1017/jfm.2019.375.

Balitsky, P. (2019) *A Numerical Investigation of the Array Effects of Wave Energy Converters With A Realistic Power Take-Off System Utilizing A Coupled Model Suite*, MSc Thesis, Universiteit Gent., Belgium.

Bosa, S. and Petti, M. (2010) 'Shallow water numerical model of the wave generated by the Vajont landslide', *Environmental Modelling and Software*, Vol. 26, No. 4, p.406–418.

Broomans, P. (2003) *Numerical Accuracy in Solutions of the Shallow-Water Equations*, MSc thesis, Delft, Netherlands.

Carrier, G.F. and Yeh, H. (2005) 'Tsunami propagation from a finite source', *Computer Modelling in Engineering and Sciences*, Vol. 10, No. 2, DOI: 10.3970/cmes.2005.010.113.

Chen, Y. and Liu P.L-F. (1995) 'Modified Boussinesq equations and associated parabolic models for water wave propagation', *Journal of Fluid Mechanics*, Vol. 288, pp.351–381, DOI: 10. 1017/S0022112095001170.

Cheviakov, A. and Zhao, P. (2024) 'Shallow Water Models and Their Analytical Properties', in: *Analytical Properties of Nonlinear Partial Differential Equations, Analytical Properties of Nonlinear Partial Differential Equations Books in Mathematics*, Vol. 10, Springer, DOI: 10.1007/978-3-031-53074-6_3.

Crowhurst, P. and Li, Z. (2013) 'Numerical Solutions of One-Dimensional Shallow Water Equations', *2013 UKSim 15th International Conference on Computer Modelling and Simulation*, Cambridge, UK, 10–12 April, pp.55–60, DOI: 10.1109/UKSim.2013.63.

Delis, A.I. and Nikolos, I.K. (2021) 'Shallow water equations in hydraulics: modeling', *Numerics and Applications Water*, Vol. 13, No. 24, p.3598, DOI: 10.3390/w13243598.

Ge, J., Wu, R. and Feng, Z. (2024) 'Solitary waves for the delayed shallow-water wave equations', *Computational and Applied Mathematics*, Vol. 43, No. 141, DOI: 10.1007/s40314-024-026550.

Hedley, J. (2009) 'A three-dimensional radiative transfer model for shallow water environments', *Optics Express*, Vol. 16, No. 26, p.21887–21902, DOI: 10.1364/OE.16.021887.

Kumar, B., Prabhu, T.S.M., Sathyan, A. and Krishnan, A. (2022) 'Chapter 36 – GLOF Early warning system: computational challenges and solutions', *Current Directions in Water Scarcity Research*, Vol. 7, pp.641–662, https://doi.org/10.1016/B978-0-323-91910-4.00036-4.

Li, G. (2024) 'Deep-water and shallow-water limits of the intermediate long wave equation', *Nonlinearity*, Vol. 37, No. 3, p.37075001, DOI: 10.1088/1361-6544/ad4843.

Lighthill, J. (2005) 'Waves in fluids', *Measurement Science and Technology*, Vol. 13, No. 9, p.1501, DOI: 10.1088/0957-0233/13/9/707.

Lyons, D.G. (2014) *Implications of Shallow Water in Numerical Simulations of A Surface Effect Ship*, MSc Thesis, Blacksburg, VA.

Maatoug, M.A. and Ayadi, M. (2016) 'Numerical simulation of the second-order Stokes theory using finite difference method', *Alexandria Engineering Journal*, Vol. 55, No. 3, pp.3005–3013, DOI: 10.1016/j.aej.2016.04.035.

Mendez, F.J. and Rueda, A. (2008) 'Progress in ocean wave forecasting', *Journal of Computational Physics*, Vol. 227, No. 7, pp.3572–3594, DOI: 10.1016/j.jcp.2007.04.029.

Mendez, F.J. and Rueda, A. (2020) '3-Wave climates: deep water to shoaling zone', *Sandy Beach Morphodynamics*, Elsevier, pp.39–59, DOI: 10.1016/B978-0-08-102927-5.00003-5.

Oliver, B. (1998) 'A shallow-water model that prevents nonlinear steepening of gravity waves', *Journal of the Atmospheric Sciences*, Vol. 55, No. 17, pp.2884–2891, DOI: 10.1088/1361-6544/ad4843.

Roberts, S.G. and Zoppou, C. (2003) 'Explicit schemes for dam-break simulations', *Journal of Hydraulic Engineering*, Vol. 129, No. 1, pp.11–34, DOI: 10.1061/(ASCE)0733-9429(2003) 129:1(11).

Stastna, M. and Steinmoeller, D. (2023) 'Rotating shallow water dynamics: an overview', *Modelling and Ecology in Fluids*, Elsevier, pp.65–90, DOI: 10.1016/B978-0-32-391244-0.00015-2.

Welahettige, P., Vaagsaether, K. and Lie, B. (2018) 'A solution method for one-dimensional shallow water equations using flux limiter centered scheme for open Venturi channels', *The Journal of Computational Multiphase Flows*, Vol. 10, No. 4, DOI: 10.1177/1757482X 18791895.

Whitham, G.B. (1974) *Linear and Nonlinear Waves*, California Institute of Technology, Wiley Editions.